CONVERGENCE STUDY OF CURRENT SAMPLING PROFILES FOR ANTENNA DESIGN IN THE PRESENCE OF ELECTRICALLY LARGE AND COMPLEX PLATFORMS USING FIT-UTD HYBRIDIZATION APPROACH

H.-T. Hsu, F.-Y. Kuo, and H.-T. Chou

Department of Communications Engineering
Communication Research Center
Yuan Ze University
Chungli 320, Taiwan

Abstract—Designing antennas in the presence of electrically large and complex structures such as cars or aircrafts has become an important issue for next generation communication systems. Based on the principle of equivalence, the hybridization approach integrating FIT-UTD techniques has shown its superiority in terms of its computing efficiency. In such approach, discrete samplings of continuous electric or magnetic field components resulted from low frequency (LF) sub-domain are required to be converted to the excitation current sources for the high frequency (HF) sub-domain. Thus, the overall accuracy of the calculation results will strongly depend on the similarities between the sampled and original field distributions with both the magnitude and phase involved. In this paper, convergence study of electric and magnetic current sampling is performed. Impact of the different sampling profiles on the overall accuracy is also investigated through numerical examples. Results reveal that convergence of the far-field radiation patterns are closely related to the sampling profiles.

1. INTRODUCTION

The advancement of wireless communication technologies has spurred drastically increasing demands for antenna operation in the presence of electrically large and complex platforms, which in turn makes it extremely challenging in terms of design for such cases. Accurate modeling of electrically large open-boundary problems using exact

---

Corresponding author: H.-T. Hsu (htbeckhsu@saturn.yzu.edu.tw).

approaches such as Finite Element Method (FEM), Finite Difference in Time Domain (FDTD), or Method of Moments (MoM) has always been challenging in electromagnetics [1–5]. The main reason is that the exact numerical methods often require discretization of the calculation domain and the physical geometry into cells with sizes comparable to the tenth (or even twentieth) of wavelength at highest calculation frequency involved.

Furthermore, even finer gridding in the vicinity of the excitation source, material interface and materials with high or nonlinear dielectric constants is necessary in order to have better convergence behavior on the computed electromagnetic fields. Over the years, lots of attentions and research efforts have been devoted to developing the gridding or meshing schemes such as perfect boundary approximation (PBA) [6] in order to improve computation efficiency. Yet, the very heavy computation load due to the small mesh sizes makes such design almost infeasible. Moreover, these problems generally involve with the analysis of small scale electromagnetic (EM) field interactions within the antenna structure and the large scale EM propagation predictions due to the couplings within the structures.

There have been several hybrid and iterative techniques developed for analyzing such problems which could not be efficiently handled by single method alone [7–11]. Specifically, low frequency (LF) techniques such as finite element method (FEM) [12], finite difference time domain (FDTD) [13] and method of moment (MoM) [13] have been shown suitable to analyze the small scale interactions within the antenna structure, but are not effective to analyze the large scale propagation problems due to the limitation of computational power. On the other hand, however, high frequency (HF) techniques [14–16] such as uniform geometrical theory of diffraction (UTD) [14], physical-optics method [17, 18], and other time domain diffraction methods [19–21] are capable of analyzing large scale propagation problems in the presence of electrically large and complex structures by using ray tracing techniques, but are not capable of analyzing the small scale interactions within the antenna because of the difficult ray tracing to achieve accurate results. The hybridization of high and low frequency techniques has been proposed and studied for decades [22–25], with most works dedicated to either assist HF techniques to increase the accuracy in predicting the wave propagations within a large structure [22] or to assist LF techniques in reducing the number of unknowns to be solved [23]. In particular, most of the works are related to either scattering problems or radiation problems associated with simple antenna structures (such as wire antennas [24, 25]). While hybrid approaches seemed to be effective for treating such challenging

problems, not much of the works, especially in terms of publicly available software, can be effectively applied to general antenna design problems resulting in a large number of repeated analysis.

Chou et al. [26] proposed a hybridization approach based on FIT-UTD techniques. The proposed approach provided a seamless integration between commercially available LF (CST MWS$^{\circledR}$ [27]) and HF (NEC-BSC [28]) codes and was successfully applied to the example of design monopole antennas on top of a vehicle. Although the proposed approach provided a simple and straightforward implementation strategy which helped to improve the computation efficiency, care must be taken when the continuous current distribution is sampled in the LF sub-domain. In such approach, discrete samplings of continuous electric or magnetic field components resulted from LF sub-domain are required to be converted as the excitation current sources for the HF sub-domain. Thus, the overall accuracy of the calculation results will strongly depend on the similarities between the sampled and original filed distributions with both the magnitude and phase involved. Tradeoff between the accuracy and efficiency is often necessary to balance the computation effort and the correctness of the results. In this paper, the convergence study of electric and magnetic current sampling is performed. Impact of the different sampling profiles on the overall accuracy and computation effort is also studied through numerical examples.

2. FIT-UTD HYBRIDIZATION APPROACH

Figure 1 shows the flow chart [26] of the procedure for the FIT-UTD approach. The main process starts from the decomposition of the complete geometry into LF and HF sub-domains. With
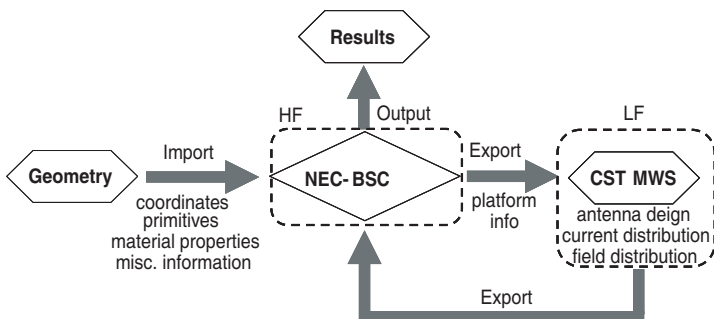
Figure 1. Flow chart of the FIT-UTD hybridization approach.

proper treatment of the artificial boundaries generated during the decomposition process, the field distribution in the near-field zone is quantized using probed field values at pre-defined locations. These probed field quantities are then converted into HF sub-domain as excitation currents.

The key concept in HF sub-domain setup is the principle of equivalence where the antenna is replaced by induced currents on a closed surface S enclosing the antenna. With negligible scattering from far-end components of the complex structure, the total fields on S are approximately the near fields radiated from the antenna designed in sub-domain. Additionally, the region inside S is perfectly electrically conducting and has a null field. Thus, the induced currents on S are magnetic and can be described as:

$$\bar{M}_s = -\hat{n} \times \bar{E}_a \tag{1}$$

where $\hat{n}$ is a unit vector normal to S and E_a is the probed near electrical field radiated from the antenna in LF sub-domain. It is noted that it is important to make the body enclosed by S electrically conducting so that the fields inside S may be retained null and the equivalent currents are directly on the surface of S during HF sub-domain analysis as required in the equivalence principle.

The induced magnetic current distributions, used as the excitation source in HF sub-domain, are related to the transmitted field as:

$$\bar{E} = -jK_m k\bar{h}\frac{e^{-jkr}}{4\pi r} \tag{2}$$

where

$$K_m\bar{h} = \hat{a}_\phi lw M_m \sin\theta F_x(\theta, \phi) F_z(\theta) F_a(\theta, \phi) \tag{3}$$

$$F_x(\theta, \phi) = \begin{cases} 1 \text{ line source} \\ \frac{\sin(\frac{1}{2}kw\cos\phi\sin\theta)}{\frac{1}{2}kw\cos\phi\sin\theta} \text{ aperture source} \end{cases} \tag{4}$$

with l and w being the physical dimensions of the current source and k being the corresponding wave number. For constant current within the discretized excitation sources as in our case, F_z can be expressed as:

$$F_z(\theta) = \frac{\sin(\frac{1}{2}kl\cos\theta)}{\frac{1}{2}kl\cos\theta} \tag{5}$$

Finally, the array pattern factor $F_a(\theta, \phi)$, is given by

$$F_a(\theta, \phi) = \sum_{n=1}^{N} I_n \exp(jk\hat{r} \cdot \bar{x}_n) \tag{6}$$

where $\bar{x}_n$ is the relative position of the nth element, I_n is the dimensionless relative weight and $\hat{r}$ is the direction of propagation.

3. NUMERICAL EXAMPLES AND CONVERGENCE ANALYSIS

As described in the previous section, the FIT-UTD approach starts with the discretization of the continuous field distributions through the applications of field probes in certain locations nearby the radiating element. Therefore, the determination of the locations of the probes will certainly have direct impact on the overall accuracy of the calculation results. In our discussions, monopole and slotted waveguide antennas are used to investigate the convergence behaviors. Since the characteristics of field variations (both in magnitude and in phase) are quite different between the two types of antennas, the conclusions drawn from such study should be comprehensively applied to other types of antennas.

Figure 2 shows the structure of interest with case (a) a quarter wavelength monopole designed at 900 MHz intended for cellular application and (b) a slotted waveguide antenna at 1.5 GHz for GPS applications. Both designs are mounted on top of the vehicle
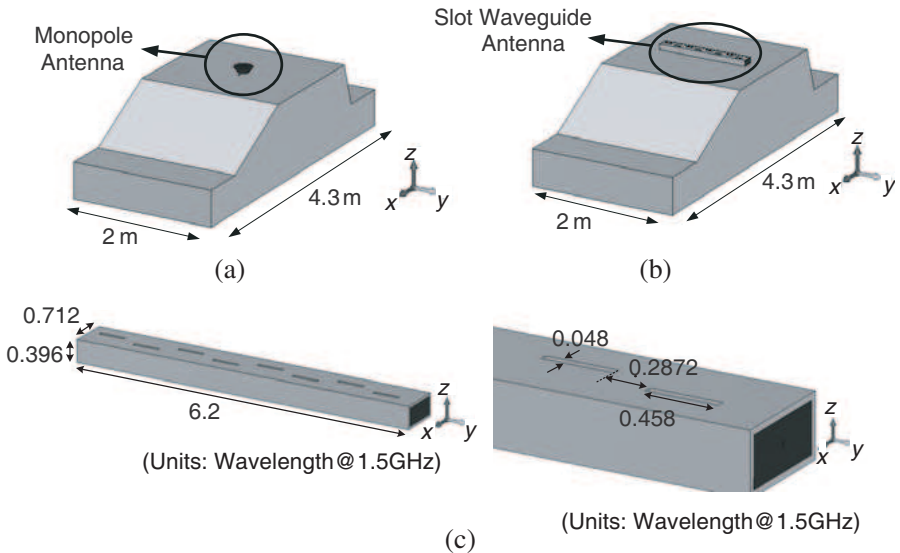
Figure 2. Illustration of the structures of interest (a) a quarter wavelength monopole antenna and (b) a slotted waveguide antenna mounted on top of a vehicle. The detailed dimensions of the slotted waveguide antenna expressed in terms of wavelength are included in (c).

with corresponding dimensions of $2\,\text{m} \times 4.3\,\text{m} \times 1.6\,\text{m}$. The detailed dimensions of the slotted waveguide antenna expressed in terms of wavelength at $1.5\,\text{GHz}$ are also included in Fig. 2(c).

FIT based CST MWS will be used as the main computation engine for LF sub-domain. Since CST is effective to analyze the small scale interactions within the antenna structure, it is nature to define a sub-domain with respect to the region in the vicinity of the antenna structure. The underlying assumption here is that the complex structure far away from the antenna does not significantly impact the antenna's electric characteristics. This condition is approximately valid for those components that are at least 2 wavelengths away from the antenna and do not directly block the antenna radiation, which generally fulfills the situations of practical applications. Thus a straightforward decomposition approach cuts the antenna vicinity region as the LF sub-domain, as illustrated in Fig. 3, for the analysis of the antenna design. The corresponding probe locations are also shown. Fig. 4 shows the corresponding HF sub-domain after the probed fields are converted to surface current distributions.

It should be noticed that only some probes are shown in Fig. 3 for illustration purposes only. In general, probes in three orthogonal directions are required to probe the three corresponding components of the magnitude and phase of the field distribution. Additionally, the probes have to be arranged in a way such that the field distributions and thus the current distributions on the enclosed surface S surrounding the antenna can be obtained as required by the principle of equivalence. As is shown in Fig. 4, each square corresponds to a uniform current element in the HF sub-domain. Therefore, the correlation on the geometry between the two sub-domains should be remained such that the probes in the LF sub-domain are at the

(a)   (b)
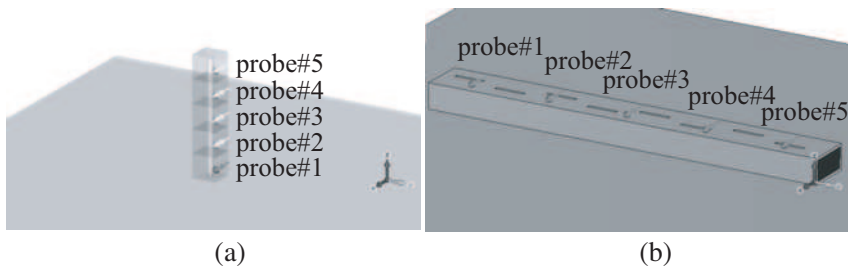
Figure 3. Decomposed structure for (a) monopole and (b) slotted waveguide with corresponding probe locations for antenna analysis in LF sub-domain.

(a)   (b)
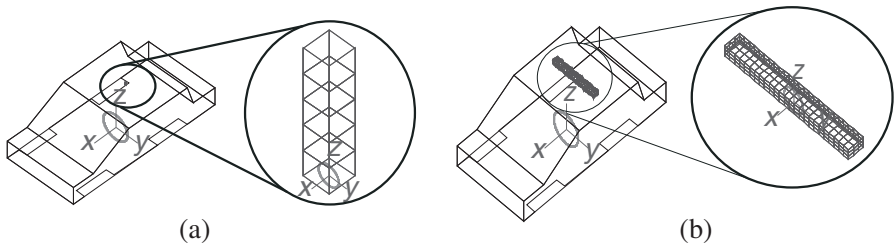
Figure 4. Corresponding HF sub-domain for (a) monopole and (b) slotted waveguide antennas showing the arrangement of the excitation currents on the enclosed surface S.

(a)

(b)
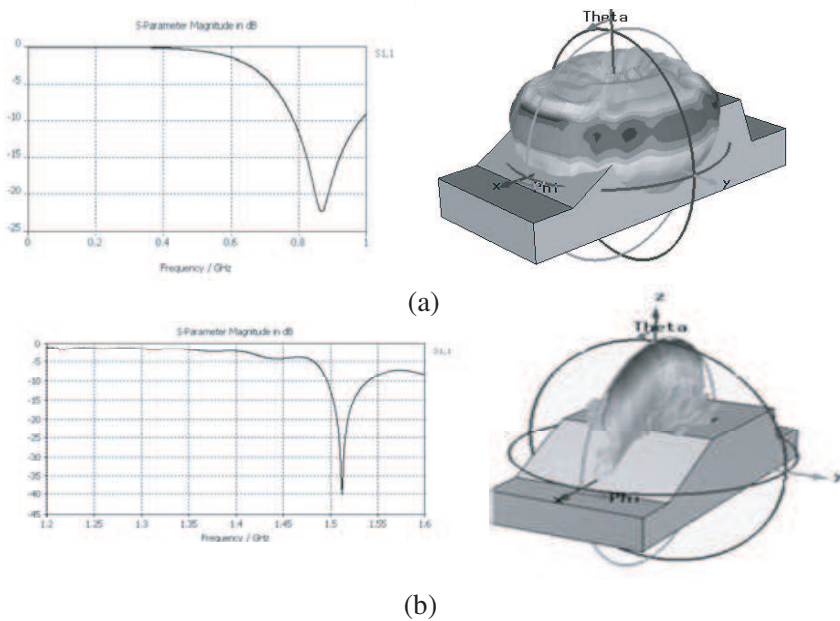
Figure 5. Simulated return loss and 3D farfield radiation patterns of (a) monopole and (b) slotted waveguide antennas using CST MWS. The results are used as for benchmarking purpose.

center of each square in the HF sub-domain. Meanwhile, the size of the decomposed LF sub-domain should be kept at least twice the wavelength away from the enclosed surface S.

Figure 5 shows the simulated return loss and 3D farfield radiation patterns for both cases using CST MWS for benchmarking purpose. For monopole case, the total number of mesh cells is 4,489,017 in this

specific case, with proper symmetry plane set to efficiently save the computational resources in terms of mesh cells and computation time which is recorded to be 65 minutes on an Intel Xeon^{TM} 3.40 GHz CPU with 3 GB RAM desktop. For slotted waveguide antenna case, a total number of 16,880,640 mesh cells are necessary since the geometry is not symmetric with respect to relevant cut planes. The corresponding simulation time for this case is 17 hours and 26 minutes on the same machine with hardware acceleration.

In LF sub-domain, the convergence of the probed magnitude and phase of the fields has to be guaranteed to ensure accurate conversion into the HF sub-domain as the excitation source. Since LF sub-domain deals mainly with the small scale interactions between the antenna and the decomposed platform, the number of mesh cells is the key parameter that governs the overall convergence. For any specific case, utilizing too many mesh cells will lead to a very long simulation time. However, if the number of mesh cells adopted is not enough, enormous error may occur which deteriorates the accuracy of the simulation results. In order to retain the computation efficiency and the accuracy of the results simultaneously, the number of mesh cells should then be determined through the convergence plots of individual probes.

To characterize the convergence behavior quantitatively without too much ambiguity, the following normalized figure of merits (for each probe) in terms of the probed magnitude and phase of the electric field are defined; assuming a total of k mesh cells between two consecutive
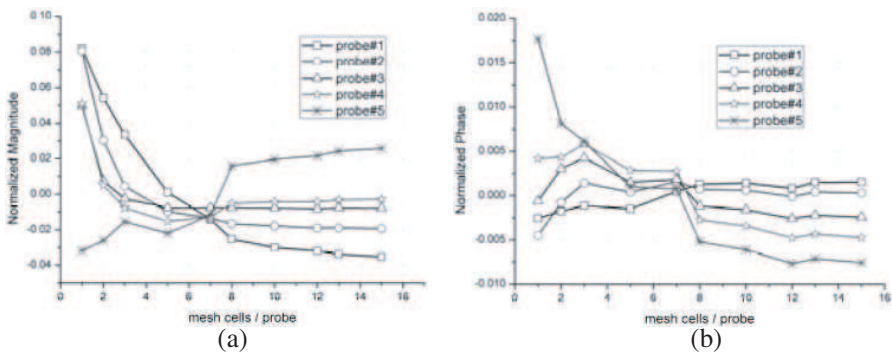
Figure 6. Plot of the convergence characteristics for (a) normalized magnitude and (b) normalized phase for the monopole antenna case with 5 current samples adopted.

probes:

$$\text{Normalized Magnitude} = \frac{\left|\vec{E}_{probe}\right| - \mu_{MAG}}{\mu_{MAG}};$$

$$\mu_{MAG} = \frac{1}{k}\sum_{i=1}^{k}|E_{probe}(i)| \tag{7a}$$

$$\text{Normalized Phase} = \frac{\measuredangle\vec{E}_{probe} - \mu_{Phase}}{\mu_{Phase}};$$

$$\mu_{phase} = \frac{1}{k}\sum_{i=1}^{k}(\measuredangle E_{probe}(i)) \tag{7b}$$

Figure 6 shows the convergence plot of the monopole antenna where the normalized magnitude and phase of each probe are plotted as functions of number of mesh cells between consecutive probes. In this case, 5 current samples were adopted to represent the continuous current distribution with a maximum number of 15 mesh cells considered between two consecutive probes. Fig. 7 shows the same plots for another case with 9 current samples adopted. Clearly, for the case of 5 current samples, both normalized figure of merits converged with more than 8 mesh cells while for the case of 9 current samples, at least 5 mesh cells were required to guarantee the convergence. Fig. 8 shows the convergence plot for slotted waveguide antenna case. A total of 25 probes along the propagation direction were adopted since a rather complicated variation in current was expected. As is observed
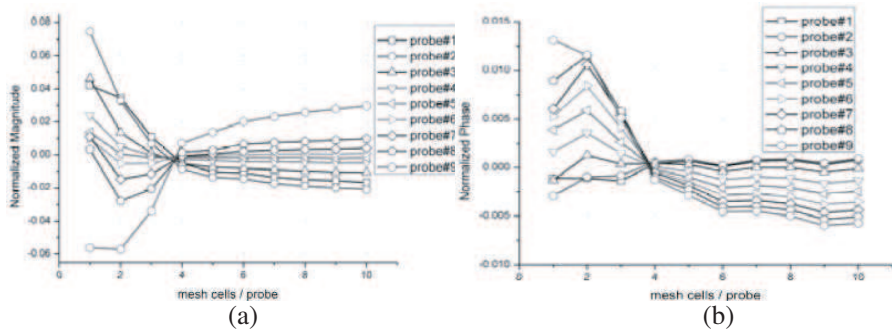
Figure 7. Plot of the convergence characteristics for (a) normalized magnitude and (b) normalized phase for the monopole antenna case with 9 current samples adopted.

in Fig. 8, a minimum of 7 mesh cell is required for convergence in probed field. It can thus be generally concluded from Figs. 6, 7 and 8 that fewer mesh cells can be used to maintain the same level of convergence with more field probes.

Once the convergence in LF sub-domain is guaranteed, the attention should then be turned into HF sub-domain where the main issue lies in the sampling profiles of the continuous current distribution. With the number of cells between the consecutive probes determined
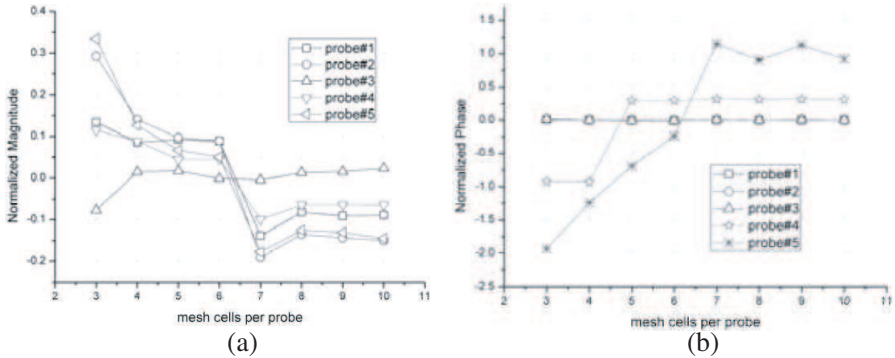
Figure 8. Plot of the convergence characteristics for (a) normalized magnitude and (b) normalized phase for the slotted waveguide antenna case with 25 current samples adopted. Only some of the probed quantities are shown for illustration.
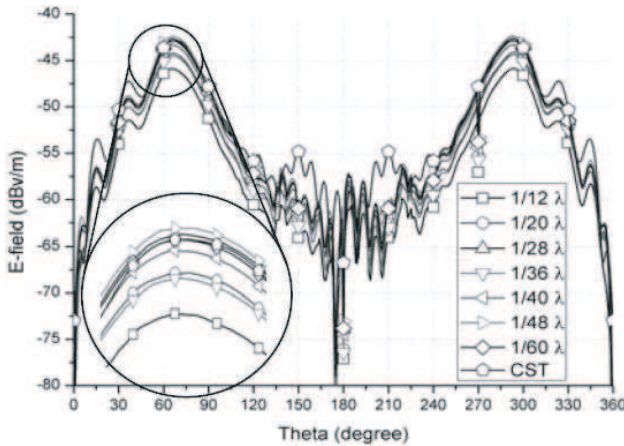
Figure 9. Convergence behavior of farfield radiation pattern for the case of monopole antenna on top of the vehicle at 900 MHz.

from the convergence analysis, total number of current samples will be varied to examine the convergence on the overall farfield radiation. Fig. 9 shows the calculated farfield radiation pattern under different sampling profiles with distance between probes (and thus the number of probes) varing from $1/12\lambda$ to $1/60\lambda$. Note that in HF sub-domain, the computation time is less than a minute while the main computational loading will be in the LF sub-domain since exact approach is used.

For the case of the slotted waveguide antenna, since the field variation is relatively drastic in the vicinity of the antenna itself, denser sampling profile implying higher number of probes should be expected. For illustration purposes, Fig. 10 shows the sampled magnitude and phase compared against the continuous distribution calculated from exact approach on x-y cut plane along y-axis under two extreme cases, 0.051λ and 0.253λ. Fig. 11 shows the computation time as a function of

(a)

(b)
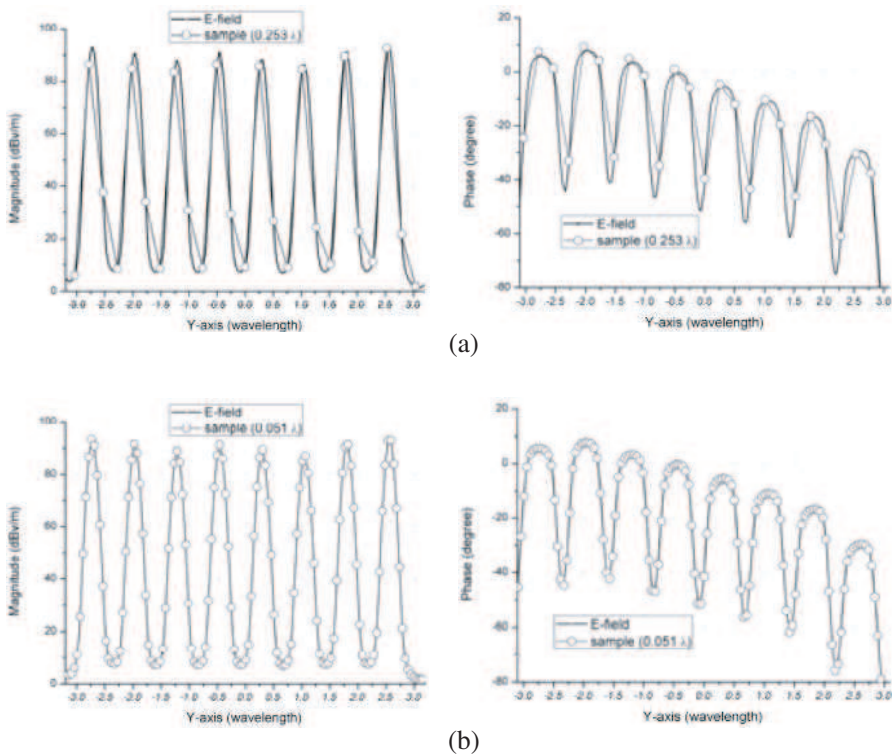
Figure 10. Comparison between the sampled and the continuous field distributions for the slotted waveguide antenna case with distance of (a) 0.253λ and (b) 0.051λ.

total number of probes for slotted waveguide antenna case. Note that the total number of probes includes all of the probes on the surfaces of the enclosed surface S. It is clear that the computation effort increases dramatically with increasing number of probes implying very dense sampling profile. Fig. 12 shows the overall convergence on the farfield radiation pattern for this case.
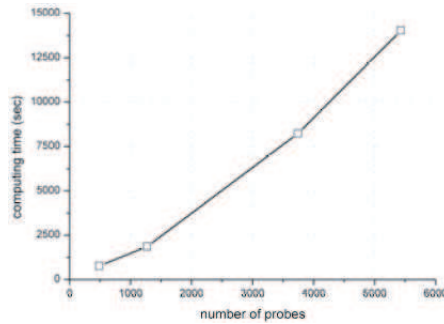
Figure 11. Computation time as a function of total number of probes on the enclosed surface S for slotted waveguide antenna case.
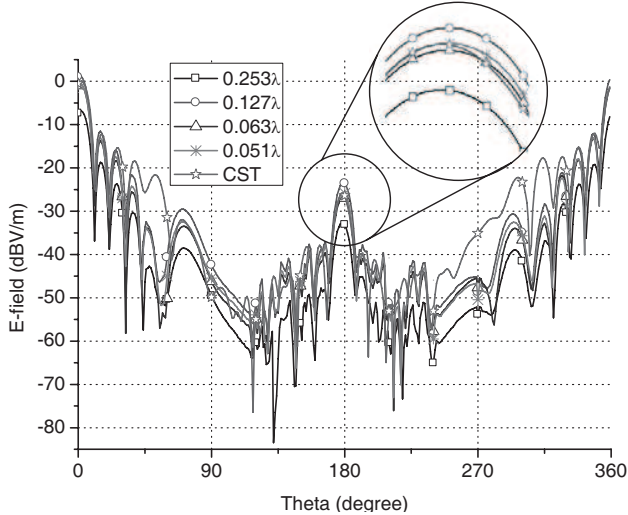
Figure 12. Overall convergence behavior of farfield radiation pattern for the case of slotted waveguide antenna on top of the vehicle at 1500 MHz.

4. CONCLUSION

FIT-UTD hybridization approach has been successfully applied to the designs of a 900 MHz monopole and a 1.5 GHz slotted waveguide antennas on top of a vehicle with overall dimensions of 2 m × 4.3 m × 1.6 m. The convergence study has also been performed to investigate the impact of the probe spacing on the overall computation accuracy compared with the benchmark results using CST MWS. Results revealed that the sampling profile strongly depends on the types of the antennas. Tradeoff between the computation time and accuracy must be made for practical design scenarios.

REFERENCES

1. Chatterjee, D., "A selective review of high-frequency techniques in computational electromagnetics," *2007 IEEE Applied Electromagnetics Conference (AEMC 2007)*, 1–4, Dec. 2007.

2. Mittra, R., "A look at some challenging problems in computational electromagnetics," (invited *paper), IEEE Antennas and Propagation Magazine*, Vol. 46, No. 5, 18–32, Oct. 2004.

3. Sarkar, T. K., S. Burintramart, N. Yilmazer, S. Hwang, Y. Zhang, A. De, and M. Salazar-Palma, "A discussion about some of the principles/practices of wireless communication under a maxwellian framework," *IEEE Transactions on Antennas and Propagation*, Vol. 54, No. 12, 3727–3745, Dec. 2006.

4. Diggavi, S., N. AI-Dhahir, A. Stamoulis, and A. R. Calderbank, "Great expectations: The value of spatial diversity in wireless networks," *Proc. IEEE*, Vol. 92, No. 2, 219–270, Feb. 2004.

5. Sarkar, T. K., Z. Ji, K. Kim, A. Medouri, and M. Salazar-Palma, "A survey of various propagation models for wireless mobile communication," *IEEE Antennas and Propagation Magazine*, Vol. 45, No. 3, 51–82, Jun. 2003.

6. Munteanu, I. and T. Weiland, "RF & microwave simulation with the finite integration technique — From component to system design," *Scientific Computing in Electrical Engineering*, Vol. 11, No. 3, 247–260, 2007.

7. Thiele, G. A., "Overview of selected hybrid methods in radiating system analysis," *Proceedings of the IEEE*, Vol. 80, 66–78, Jan. 1992.

8. Han, D.-H., A. C. Polycarpou, and C. A. Balanis, "FEM-based hybrid methods for the analysis of antennas on electrically

large structures," *2000 IEEE Radio and Wireless Conference, RAWCON 2000*, 59–61, Sep. 2000.

9. Oğuzer, T. and A. Altintas, "Analysis of the nonconcentric reflector anatenna-in-radome system by the iterative reflector antenna and radome interaction," *Journal of Electromagnetic Waves and Applications*, Vol. 21, No. 1, 57–70, 2007.

10. Zhang, P. F. and S. X. Gong, "Improvement on the forward-backward iterative physical optics algorithm applied to computing the RCS of large open-ended cavities," *Journal of Electromagnetic Waves and Applications*, Vol. 21, No. 4, 457–469, 2007.

11. Betzios, P. V., I. S. Karanasiou, and N. K. Uzunoglu, "Analysis of a dielectric resonator antenna by applying a combined semi-analytical method and simulation," *Journal of Electromagnetic Waves and Applications*, Vol. 21, No. 14, 1983–1994, 2007.

12. Volakis, J. L., A. Chatterjee, and L. C. Kempel, *Finite Element Method for Electromagnetics: Antennas, Microwave Circuits, and Scattering Applications*, IEEE Press and Oxford University Press, New York, 368, 1998.

13. Taflove, A., "Application of the finite-difference time-domain method to sinusoidal steady state electromagnetic penetration problems," *Electromagnetic Compatibility, IEEE Transaction*, Vol. 22, 191–202, 1980.

14. Harrington, F. F., *Computation by Moment Methods*, Macmillan, New York, 1968.

15. Kouyoumjian, R. G. and P. H. Pathak, "A uniform geometrical theory of diffraction for an edge in a perfectly conducting surface," *Proceedings of the IEEE*, Vol. 62, No. 11, 1448–1461, Nov. 1974.

16. Ufimtsev, P. Y., *Method of Edge Waves in the Physical Theory of Diffraction*, Wiley-IEEE Press, Feb. 16, 2007.

17. Tiberio, R., S. Maci, and A. Toccafondi, "An incremental theory of diffraction: Electromagnetic formulation," *IEEE Transactions on Antennas and Propagation*, Vol. 43, No. 1, 87–96, Jan. 1995.

18. Chen, M., Y. Zhang, and C. H. Liang, "Calculation of the field distribution near electrically large nurbs surfaces with physical-optics method," *Journal of Electromagnetic Waves and Applications*, Vol. 19, No. 11, 1511–1524, 2005.

19. Zhang, P. F. and S. X. Gong, "Improvement on the forward-backward iterative physical optics algorithm applied to computing the rcs of large open-ended cavities," *Journal of Electromagnetic Waves and Applications*, Vol. 21, No. 21, 457–469, 2007.

20. Attiya, A. M., E. El-Diwany, A. M. Shaarawi, and I. M. Besieris,

"A time domain incremental theory of diffraction: Scattering of electromagnetic pulsed plane waves," *Progress In Electromagnetics Research*, PIER 44, 81–101, 2004.

21. Attiya, A. M., E. El-Diwany, A. M. Shaarawi, and I. M. Besieris, "Scattering of X-waves from a circular disk using a time domain incremental theory of diffraction," *Progress In Electromagnetics Research*, PIER 44, 103–129, 2004.

22. Thiele, G. A. and T. H. Newhouse, "A hybrid technique for combining moment methods with the geometrical theory of diffraction," *IEEE Transactions on Antennas and Propagation*, Vol. 23, No. 1, Jan. 1975.

23. Burnside, W., C. Yu, and R. Marhefka, "A technique to combine the geometrical theory of diffraction and the moment method," *IEEE Transactions on Antennas and Propagation*, Vol. 23, No. 4, 551–558, Jul. 1975.

24. Fourie, A. and D. Nitch, "SuperNEC: Antenna and indoor-propagation simulation program," *IEEE Antennas and Propagation Magazine*, Vol. 42, No. 3, 31–48, Jun. 2000.

25. Davidson, D. B., I. P. Theron, U. Jakobus, F. M. Landstorfer, F. J. C. Meyer, J. Mostert, and J. J. Van Tonder, "Recent progress on the antenna simulation program FEKO," *Communications and Signal Processing, 1998. COMSIG'98. Proceedings of the 1998 South African Symposium on*, 427–430, Sep. 7–8, 1998.

26. Chou, H.-T. and H.-T. Hsu, "Hybridization of simulation codes based on numerical high and low frequency techniques for the efficient antenna design in the presence of electrically large and complex structures," *Progress In Electromagnetics Research*, PIER 78, 173–187, 2008.

27. CST Studio Suite 2009 User's Manual, CST Computation Simulation Technology, www.cst.com.

28. NEC-BSC version 4.2 User's Manual, The Ohio State University, Jun. 2000.